M. de Lucia

C. Lanfranchi

Dipartimento di Energetica,
Università degli Studi di Firenze,
Via di Santa Marta, 3,
50139 Firenze, Italy

An Infrared Pyrometry System for Monitoring Gas Turbine Blades: Development of a Computer Model and Experimental Results

This work describes the development of a computer modeling system for infrared pyrometry measurement of gas turbine blade temperature. The model accurately evaluates apparent target emissivity and temperature on the basis of the radiation heat fluxes exchanged at steady-state conditions. Experimental testing conducted on gas turbine models in a controlled-temperature furnace has shown that the reliability of the target emissivity prediction effectively reduces one of the major causes of error in infrared pyrometry.

Introduction

The thermal efficiency of gas turbine engines has been steadily climbing over the past two decades. However, the tradeoff for greater efficiency has been higher and higher gas temperatures at turbine inlet and increasingly severe combinations of temperature and stress on the rotating components.

The capacity to measure temperature accurately in the turbine's rotating components has thus become an integral part of the development and monitoring phases of these machines (Schulemberg and Bals, 1987). Currently, two methods are employed: the direct contact method, utilizing sensors placed in direct contact with the moving parts, together with telemetry or slip rings, and the noncontacting method, utilizing instruments such as optical pyrometers (Beynon, 1982; Scotto and Eismeier, 1980).

Optical pyrometers measure the radiation emitted by a body according to its temperature. The two major sources of error in temperature measurement are optical contamination (Love, 1988; Kirby et al., 1986) and inaccurate evaluation of the target emissivity (Kirby et al., 1986; Benyon, 1981; Douglas, 1980). The proposed system supplies apparent emissivity and temperature values in real time with an error within 1 percent.

The theoretical basis underlying radiative heat transfer is the emission or radiance of the so-called blackbody expressed by Planck's law:

$$L_b(\lambda, T) = \frac{c_1}{\lambda^5(e^{c_2/\lambda T} - 1)} \tag{1}$$

An approximation often used to simplify the calculation of radiative heat transfer is Wien's law, whose validity is limited by the condition $(\lambda T) \ll c_2$, so that

$$L_b(\lambda, T) = \frac{c_1}{\lambda^5} e^{-c_2/\lambda T} \tag{2}$$

Real surfaces behave quite differently from ideal. Hence, the reliability of the temperature measurements is related to the degree of accuracy achieved in evaluating the emissivity parameter. The following equation:

$$\frac{dT}{T} = -\frac{\lambda T}{c_2}\frac{d\epsilon}{\epsilon} \tag{3}$$

shows that the error on the temperature caused by inaccuracy in the spectral emissivity for a given radiance temperature can be unacceptable, even when the emissivity error is slight.

A useful parameter in evaluating the transfer of radiation heat, and consequently the actual temperature, is the target apparent emissivity ϵ_a. This can be defined (Ono, 1988) as the ratio of the target exitent radiation[1] to blackbody radiance at the target temperature

$$\epsilon_a = \frac{L_{ex}(\lambda, T_t)}{L_b(\lambda, T_t)} \tag{4}$$

Hence, the knowledge of the target apparent emissivity ϵ_a, being dependent on the surrounding environment and not only on the real surface's physical properties, is critical in radiometric measurements.

Computer Modeling

Our aim in developing the computer model was to evaluate as accurately as possible the apparent emissivity in relation to the geometries, materials, and temperatures of the various components. The actual pyrometer target temperature is cal-

Contributed by the International Gas Turbine Institute and presented at the 37th International Gas Turbine and Aeroengine Congress and Exposition, Cologne, Germany, June 1–4, 1992. Manuscript received by the International Gas Turbine Institute February 4, 1992. Paper No. 92-GT-80. Associate Technical Editor: L. S. Langston.

[1]Exitent radiation = emitted + reflected radiation as defined by DeWitt and Incropera (1988). It is also called "radiosity" by Sparrow and Cess (1978), and others.

culated on the basis of the total energy transferred by radiation from the target to the surrounding bodies. The following assumptions were made:

1 Radiative heat transfer was assumed at steady-state conditions.

2 All radiances, powers, energies, and emissivities were assumed spectral, allowing evaluation at the pyrometer's constant wavelength.

3 The surfaces were assumed isothermal and gray, that is, as emitting and reflecting diffusely.

4 The surfaces were assumed to form a cavity, that is, without radiative heat transfer to the environment.

Each surface transfers heat via radiation to the other $n-1$ surfaces. The power balance of the generic surface i at steady-state conditions is

$$P_{ex_i} = P_{em_i} + P_{r_i} \tag{5}$$

with a reflected power of

$$P_{r_i} = (1-\epsilon_i) \sum_{j=1}^{n} P_{ex_{ij}} \tag{6}$$

where $P_{ex_{ij}}$ is the exitent power from surface j reaching surface i. This term can be expressed by the angle factors F_{ij}, i.e., the percentage of exitent power from j reaching i

$$F_{ij} = \frac{P_{ex_{ij}}}{P_{ex_j}} \tag{7}$$

The adimensional angle factors, related only to the geometric parameters, can be calculated according to Sparrow and Cess (1978).

Substituting radiances for the powers and using the calculated angle factors, we can rewrite the power balance, Eq. (5):

$$L_{ex_i} = L_{em_i} + \frac{(1-\epsilon_i)}{A_i} \sum_{j=1}^{n} (A_j L_{ex_j} F_{ij}) \tag{8}$$

which is a linear system of n equations in n unknowns, L_{ex_i}, with radiances L_{em_i} as its known terms. Assuming surface k as the target, we can determine the temperatures of the other $n-1$ surfaces by direct measurement or by theoretical correlations and acquire the temperature read by the pyrometer at the set emissivity. We can then calculate the target radiance by solving an n-dimensional linear system (Sparrow and Cess, 1978). It should, however, be recalled that the pyrometer temperature, due to the uncertainty of the set emissivity, can deviate notably from the target temperature. Actually, we can directly calculate the target exitent radiance L_{ex_k} with the pyrometer temperature T_{pyr}, whereas the unknown is the target's blackbody radiance L_{b_k} used to determine the actual target temperature. The kth equation of the linear system thus becomes

$$L_{b_k} = \frac{1}{\epsilon_k}\left[L_{ex_k} - \frac{(1-\epsilon_k)}{A_k} \sum_{j=1}^{n} (A_j L_{ex_j} F_{kj}) \right] \tag{9}$$

Since the other $n-1$ equations are independent of the unknown L_{b_k}, we can later solve Eq. (9) separately. The linear system reduces to a system $(n-1) \times (n-1)$ in the unknowns L_{ex_i}, $i \neq k$. The matrix of the linear system (8) $[B_{ij}]$ is defined as

$$B_{ij} = \delta_{ij} - \frac{(1-\epsilon_i)}{A_i} A_j F_{ij} \quad \begin{matrix} i, j = 1, 2, \ldots, n \\ i, j \neq k \end{matrix} \tag{10}$$

with the known term

$$C_i = \epsilon_i L_{b_i} + \frac{(1-\epsilon_i)}{A_i} A_k L_{ex_k} F_{ik} \quad \begin{matrix} i = 1, 2, \ldots, n \\ i \neq k \end{matrix} \tag{11}$$

The system may be written in matrix form

$$[B] \times [L_{ex}] = [C] \tag{12}$$

with matrix $[B]$ independent of temperature once the target has been defined. The matrix calculation is performed only once, since the geometry and physical constants of the problem are known. Having determined radiances L_{ex_i} and having substituted them in Eq. (9), we can calculate the target blackbody radiance L_{b_k} and thus the actual temperature by inverting Planck's equation. The target apparent emissivity ϵ_{ak} results

$$\epsilon_{a_k} = \frac{L_{ex_k}}{L_{b_k}} \tag{13}$$

Physical Models

Two physical models of diverse complexity were developed and tested: one, simplified, to test the data acquisition system, the sighting system, and the computer model, and one, more complex, configured to duplicate actual machine operation as closely as possible.

Simple Model. The simplified model consisted of an inconel cylinder with an emissivity of 0.83 positioned inside a cavity lined with refractory material with an emissivity of 0.3. The pyrometer target was a 4-mm circular surface in the middle of the cylinder's upper surface. The model was instrumented with 11 thermocouples: Eight were positioned on a radius 12 mm from the target center (four on the surface and four 1 mm below the surface), two were positioned at the target edge, and one was positioned on the refractory wall. The cylinder was designed with special internal cavities to obtain an isothermal upper surface even during cooling. Testing was conducted with a rhodium-coated mirror to deviate the line-of-sight by 90 deg and with no mirror.

Nomenclature

A = surface area, m^2
a = distance, m
c_1 = first radiation constant, $W\ \mu m^4 m^{-2} sr^{-1}$
c_2 = second radiation constant, μm K
F = angle factor
h = length, m
L = radiance, $Wm^{-2}sr^{-1}\ \mu m^{-1}$
l = length, m
P = radiant power, $W\ \mu m^{-1}$
s = width, m
T = temperature, K
x = spatial coordinate, m
γ = angle between perpendicular and the y axis, rad
δ_{ij} = Kronecker delta
ϵ = emissivity
λ = wavelength, μm
ρ = reflectance
φ = angular width, rad

Subscripts

a = apparent
b = blackbody conditions
em = emittent
ex = exitent
m = mirror
pyr = pyrometer
r = reflected
ref = refractory
t = target (actual)
tc = target (calculated)

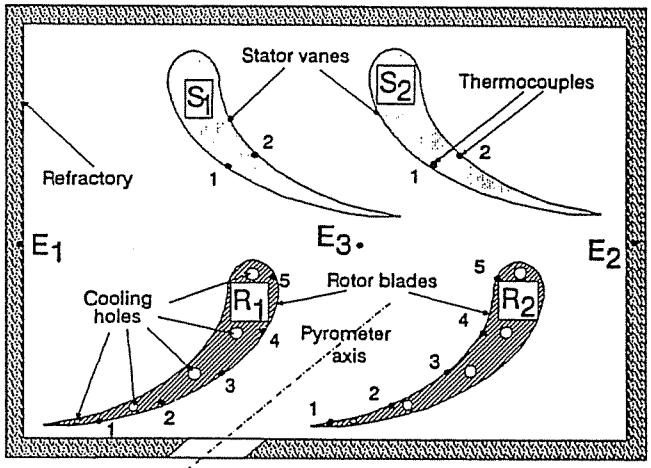

Fig. 1 Schematic of the experimental model

Only two surfaces, the cylinder and the refractory surface, were considered in modeling with constant, homogeneous properties for both. In this way, the angle factor calculation was simplified so that we could avoid having to solve the linear system. We were thus able to perform a check on how the system worked, having explicated the apparent emissivity in relation to the actual cylinder radiance L_{ex_1} and the blackbody refractory radiance L_{b_2} as

$$\epsilon_{a_1} = \frac{1}{a - b\dfrac{L_{b_2}}{L_{ex_1}}} \tag{14}$$

where 1 is the target index, 2 is the refractory index, and the constants a and b are

$$a = \frac{1}{\epsilon_1}\left[1 - (1-\epsilon_1)F_{11} - \frac{(1-\epsilon_1)(1-\epsilon_2)F_{12}F_{21}}{1-(1-\epsilon_2)F_{22}}\right]$$

$$b = \frac{\epsilon_2(1-\epsilon_1)F_{12}}{\epsilon_1[1-(1-\epsilon_2)F_{22}]}\frac{A_2}{A_1}$$

Complex Model. The complex model (Fig. 1) was comprised of a plate sustaining two stator vanes and two rotor blades placed inside a cavity formed by a refractory shield. The blades were arranged to reproduce actual machine geometric conditions as closely as possible. The blade surfaces were of oxidated inconel with an emissivity of 0.83. As in the simple model, the cavity was lined in a refractory material with an emissivity of 0.3. Five thermocouples were installed on each blade (suction side of blade $R1$ and pressure side of blade $R2$): two on each (uncooled) stator vane ($S1$ and $S2$), two on the refractory material ($E1$ and $E2$), and one in the environmental space ($E3$). The blades were cooled by an airflow from outside, which, after passing through the cooling holes, was exhausted outside through a duct. A control system was installed so that the temperature of the rotor blades could be varied separately.

In order to reproduce the actual machine layout of the sighting system, we used a mirror to deviate the line-of-sight. The mirror required constant cooling and air purging to maintain high reflectivity and low emissivity. In the sighting system, a second cooling airflow (Fig. 2) was routed over the pyrometer's jacket to the optical components prior to reaching the mirror. Since the flow of cooling air inside the controlled-temperature furnace had to be avoided, an outer jacket was attached to a vacuum pump to keep the air from reaching the target and altering the temperature distribution.

The following test equipment was selected:

(*a*) a Land high-temperature infrared pyrometer with $\lambda = 1$ μm

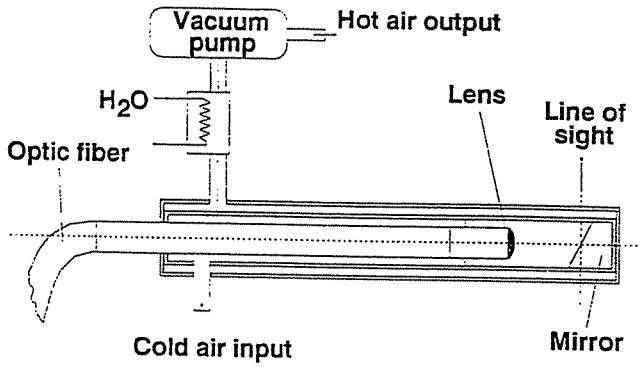

Fig. 2 Schematic of the sighting tube and cooling system

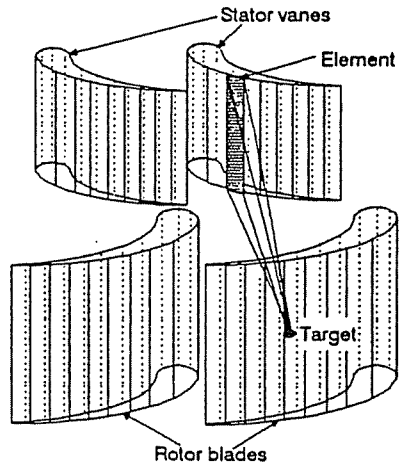

Fig. 3 Model discretization

(*b*) a support-sighting system (Fig. 2) including a mirror with a rhodium surface to provide the 90-deg deviation to the line-of-sight

(*c*) a Hewlett-Packard data acquisition system

(*d*) a dedicated personal computer for processing the data from the data acquisition system and evaluating ϵ_a in real time

(*f*) a controlled-temperature electric furnace (0–1200°C)

The blades (Fig. 3) were modeled as no-twist, two-dimensional bodies with a cross section equal to the blade midheight section and discretized with 22 connected points. A computer program was written to calculate the angle factor with finer discretization. Elementary isothermal rectangular elements were used in discretizing the blade surfaces and circular sectors and rectangles for the blade surrounding area (refractory surfaces). As the calculation of the angle factors is wholly dependent on system geometry and therefore extremely complicated, we chose an analytical method that would increase calculation accuracy and speed. The angle factor between two thin rectangular surfaces with perpendiculars parallel to the same plane (Fig. 4) can be expressed

$$F = \frac{s_1 s_2 \cos\gamma_1 \cos\gamma_2}{2\pi A a}\left[(x_1 + h_1 - x_2)\tan^{-1}\left(\frac{x_1 + h_1 - x_2}{a}\right)\right.$$
$$+ (x_1 - h_2 - x_2)\tan^{-1}\left(\frac{x_1 - h_2 - x_2}{a}\right) - (x_1 - x_2)\tan^{-1}\left(\frac{x_1 - x_2}{a}\right)$$
$$\left. - (x_1 + h_1 - x_2 - h_2)\tan^{-1}\left(\frac{x_1 + h_1 - x_2 - h_2}{a}\right)\right] \tag{15}$$

while the angle factor between a thin rectangular surface and a crown sector in perpendicular planes (Fig. 5) is

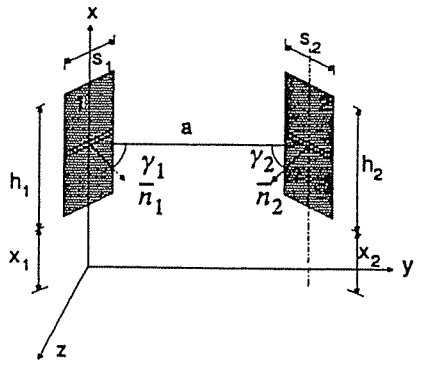

Fig. 4 Geometry for the angle factor calculation for a two-rectangle system

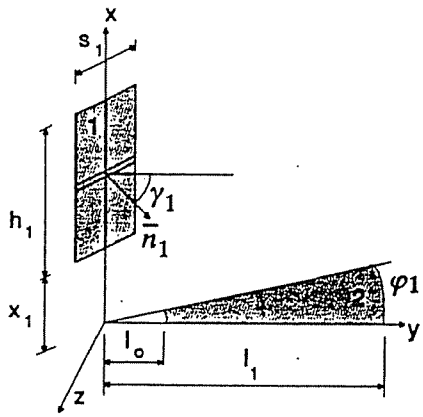

Fig. 5 Geometry for the angle factor calculation for a rectangle- and circular-sector system

$$F=\frac{s_1}{2\pi A}\left[\sin(\gamma_1+\varphi_1)-\sin(\gamma_1)\right]\left[x_1\tan^{-1}\left(\frac{l_0}{x_1}\right)-x_1\tan^{-1}\left(\frac{l_1}{x_1}\right)\right.$$

$$\left.-(x_1+h_1)\tan^{-1}\left(\frac{l_0}{x_1+h_1}\right)+(x_1+h_1)\tan^{-1}\left(\frac{l_1}{x_1+h_1}\right)\right] \quad (16)$$

Additionally, since the angle factors between elements may also be combined (Sparrow and Cess, 1978), the system for the final solution may be notably reduced to a minimum related to the number of data available. The blade temperature distribution can be derived from theoretical or experimental values, which in our case consisted of the 17 thermocouple measurements.

Experimental Results

Experimental testing was performed at furnace temperatures between 600–1000°C. The tests on the simple model designed to validate the reliability of the mathematical model and approximations were also useful in developing the mirror cooling and sighting-support systems.

Simple Model. Figure 6 shows the calculated and experimental results for a test considered among the most significant. Close agreement between the calculated and experimental temperatures is evident, with the relative error below 0.5 percent. The fact that the set emissivity was varied between 0.8–1.1 had no negative effect on the calculation of the target temperature.

Complex Model. The results were satisfactory under all test conditions, i.e., with variations in the target surface, temperature, blade cooling air flow rate, as well as with air purging. In all cases, the error was limited to within 1 percent and in

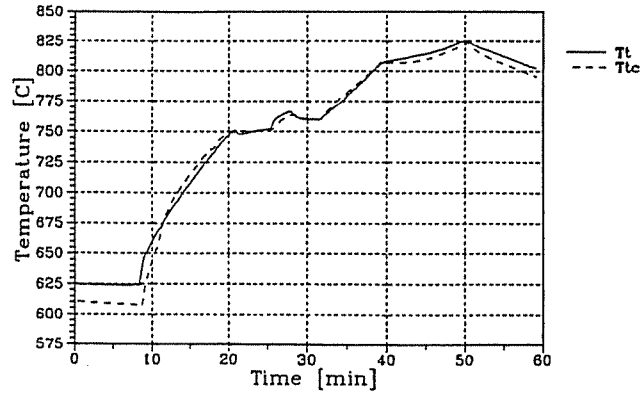

Fig. 6 Simple model: experimental (T_t) and calculated (T_{tc}) target temperatures

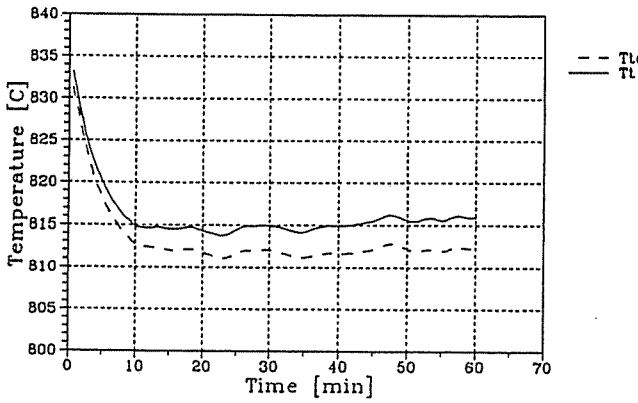

Fig. 7 Complex model: experimental (T_t) and calculated (T_{tc}) target temperatures

many cases even fell below 0.5 percent. Although the model was designed for steady-state calculations, testing was also performed over a transient. The results were positive for slight temperature variations in time, with the error rate peaking steeply only for the more abrupt transients.

A deterioration in mirror performance was often encountered even during a single test period (1–2 h). This was due to the limitations of our cooling and purge systems, as well as to the high operating temperature of the mirror (100–150°C below target temperature). Mirror performance varied in relation to both operating temperature and exposure time: In high-temperature testing ($T>900$°C) mirror life was no longer than 2–3 hours, increasing only when the temperature was decreased. The normal mirror reflectance value of 0.79 ± 0.01, supplied by the manufacturer, was found to be correct only at favorable conditions, i.e., at ambient temperature and after polishing. Experimental calibration tests proved that mirror reflectance decay was nearly linear with the test temperature exposure time. Therefore, throughout testing, we assumed a constant mean mirror reflectance ρ_m of 0.76 ± 0.01, calculated averaging the actual mirror reflectance over two hours' exposure time at 750°C. This accounts for the attenuation of the reflected signal due to the deterioration in mirror performance.

The results of a test performed at 860°C are shown in Figs. 7–9. The temperature of the target (the area around thermocouple 3 on blade $R2$) was found to be 45°C cooler than the furnace, whereas the stator vanes were between 20–35°C hotter on the target. The temperature irregularity on blade $R2$ was 15°C. Figure 7 shows that the calculated and experimental target temperatures were in good agreement throughout testing, with a relative error $(T_{tc}-T_t)/T_t\cdot 100$ that tends to increase in time up to a maximum (in absolute terms) of 0.45 percent (Fig. 8). The initial transient was caused by the opening of the blade cooling air valve. (Note that values higher than the 45°C set here were used in other tests.) Figure 9 shows that the calculated apparent emissivity remained constant at 1.073.

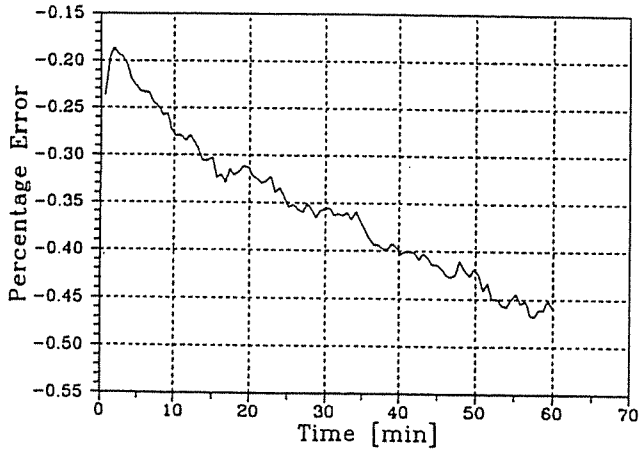

Fig. 8 Calculated target temperature error (percent)

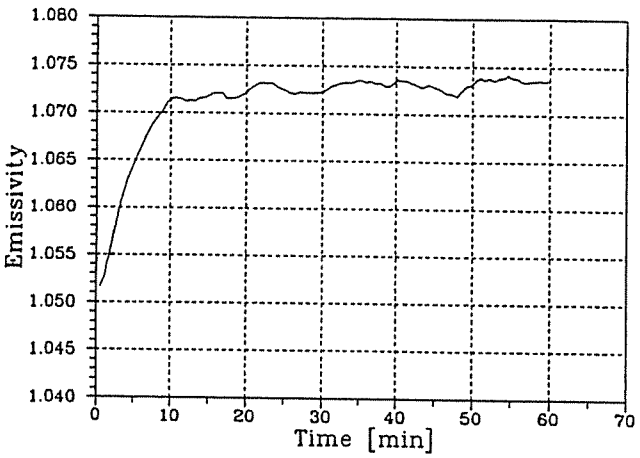

Fig. 9 Calculated target emissivity

Sensitivity and Error Analysis

The measuring error and its calculation-induced amplification were analyzed in order to validate the model's reliability. Having assumed a maximum error of 0.75 percent for each thermocouple and ±3°C for the pyrometer, we computed the maximum error of ±4°C on the calculated temperature both for the simplified and complex models—a more than acceptable error for the type of application under investigation.

Simple Model. A sensitivity analysis was performed to verify the versatility of the model. Since only two surfaces, the cylinder and the refractory surface, were considered, the calculation was appreciably simplified.

The sensitivity curves plotted in Fig. 10 show how the target temperature error depends on the refractory temperature uncertainty for various target temperatures and for a refractory-target temperature difference ($T_{ref} - T_t$) of 100°C. If the error on the refractory surface temperature is negative, the error on the calculation of the target temperature is small. Conversely, a positive refractory temperature error causes an appreciable increase in the target temperature calculation error: the lower the target temperature, the more marked the increase. Therefore, an underestimation causes a smaller error than an overestimation. The same calculations were performed for various values of the refractory-target temperature difference ($T_{ref} - T_t$) (not illustrated here). As this parameter decreases, i.e., as the system tends to isothermal conditions, the target temperature error approaches zero.

Complex Model. Since, in applying such temperature measurement systems, one of the major uncertainties is the temperature to assign to the elements used to discretize the model, we assumed in the sensitivity analysis a maximum random error of 50°C on each measured temperature, with a higher probability of underestimation (75 percent of the cases) than overestimation. Due to the assumption of random error distribution, the calculation error was extremely variable, without, however, exceeding an average of 1.5 percent. Not surprisingly, the error decreased as the number of elements used in discretization increased.

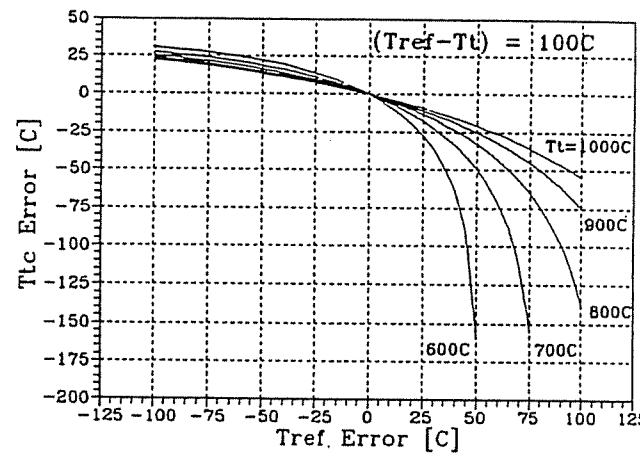

Fig. 10 Target temperature (T_t) error versus refractory surface temperature (T_{ref}) error

Conclusions

Experimental testing on models of gas turbine components has confirmed that the proposed system furnishes accurate temperature measurements at steady- or near-steady-state conditions and regardless of the emissivity set on the pyrometer. The proposed method furnishes an accurate evaluation of emissivity and thus of temperature, which in this way is univocally defined. This means that the temperature measurement can be made by an operator without special training or skills. By contrast, the sensitivity required for the discretization and calculation of the angle factors calls for more sophistication (even though this operation need only be performed once if the system geometry has not been changed in the meantime).

Obviously, the calculation accuracy is related to the degree of accuracy with which we know the parameters regarding our operating environments. The method as presented in this work has been applied to models on which it is possible to measure the temperatures of all of the surfaces surrounding the target. Hence, it must be modified before being applied to real machines in which temperatures are obtained by empiric estimates or, better still, by multiple pyrometer measurements. The target temperature can then be calculated by solving coupled sets of linear equations. This application, now under development, will be presented in a forthcoming work.

Acknowledgments

The authors are grateful to Pierluigi Nava of NuovoPignone and Francesco Carleo for their help in carrying out the experimental program and to Professor Ennio Carnevale for his invaluable support. This work was partially funded by NuovoPignone S.p.A.

References

Beynon, T. G. R., 1981, "Turbine Pyrometry—An Equipment Manufacturer's Viewpoint," ASME Paper No. 81-GT-136.

Beynon, T. G. R., 1982, "Infrared Radiation Thermometry Applied to the Development and Control of Gas Turbine Engines," *Proceedings, International*